catalysts

MDPI

Article

Effect of Transition Metal Additives on the Catalytic Performance of Cu–Mn/SAPO-34 for Selective Catalytic Reduction of NO with NH_3 at Low Temperature

Guofu Liu [1,2,†], Wenjie Zhang [1,†], Pengfei He [3], Dekui Shen [1,2,*], Chunfei Wu [4] and Chenghong Gong [5]

1 Key Laboratory of Energy Thermal Conversion and Control of Ministry of Education, School of Energy and Environment, Southeast University, Nanjing 210096, China
2 Nanjing Blinked Institute of Energy Saving and Environmental Protection, Nanjing 211500, China
3 Jiangsu Frontier Electric Power Technology Co., Ltd., Nanjing 211102, China
4 School of Chemistry and Chemical Engineering, Queen's University Belfast, Belfast BT7 1NN, UK
5 Jiangsu Yanxin SCI-TECH Co., Ltd., Wuxi 214426, China
* Correspondence: 101011398@seu.edu.cn; Tel.: +86-025-83794744
† These two authors contribute equally to the manuscript.

Received: 24 July 2019; Accepted: 9 August 2019; Published: 13 August 2019

Abstract: The adsorption of NO, NH_3, H_2O, and SO_2 gaseous molecules on different transition metal oxides was studied based on density function theory (DFT), and three better-performing transition metal elements (Fe, Co, and Ce) were selected. Cu–Mn/SAPO-34 catalysts were prepared by impregnation method and then modified by the selected transition metals (Fe, Co, and Ce); the SO_2 resistance experiments and characterizations including Brunner–Emmet–Teller (BET), X-ray Diffraction (XRD), Scanning Electronic Microscopy (SEM), and thermal gravity analysis (TG)-differential thermal gravity (DTG) before and after SO_2 poisoning were conducted. The results showed that the deactivation of the Cu–Mn/SAPO-34 catalyst is ascribed to the deposition of lots of ammonium sulfates on the surface, depositing on the active sites and inhibiting the adsorption of NH_3. After the modification of Fe, Co, and Ce oxides, the SO_2 resistance of the modified Cu–Mn/SAPO-34 catalyst was significantly enhanced due to the less formation of ammonium sulfates. Among all these modified Cu–Mn/SAPO-34 catalysts, the Cu–Mn–Ce/SAPO-34 exhibited the highest SO_2 resistance owing to the decreased decomposition temperature and the trapper of ceria for capturing SO_2 to form $Ce(SO_4)_2$, further inhibiting the deposition of ammonium sulfates.

Keywords: selective catalytic reduction; DFT; transition metal additives; SO_2

1. Introduction

Selective catalytic reduction with NH_3 (NH_3-SCR) is considered as one of the most efficient techniques to control NO_x emissions [1,2]. V_2O_5-based catalyst is commonly adopted for its high activity for NO reduction and low sensitivity towards SO_2 poisoning [2]. However, several issues such as the high reaction temperature (300–400 °C), high cost, the toxicity and higher oxidizability of vanadia, and low N_2 selectivity limit its applications [3]. Therefore, significant efforts have been made to develop low-temperature SCR catalysts, which will be applied in industrial boiler systems to remove NO_x below 250 °C, contributing to the low energy consumption and easy retrofit for flue gas cleaning. Many SCR catalysts containing transition metals (Mn, Cu, Fe, Ce, Co, and V) have been reported to be effective in low-temperature SCR reaction [4–8]. Among all these transition metals, MnO_2 is found to

be an important oxide component in the SCR reaction, due to the various types of labile oxygen and high oxygen-storage capacity [9]. CuO is found to be highly resistant to SO_2 in the low-temperature SCR reaction due to the activity of $CuSO_4$ [10]. It is reported that the Mn-Cu/SAPO-34 catalyst displays remarkable hydrothermal stability and good SCR activity in a broad temperature range [11–13].

It is well accepted that the application of low-temperature SCR catalyst relies not only on the high SCR activity, but also the superior SO_2 resistance due to the fact that the exhaust from the industrial boiler system contains a good amount of SO_2. However, Mn-based catalysts are proven to be sensitive to SO_2 poisoning. Two main deactivation routes are widely reported. Firstly, SO_2 can be oxidized to SO_3, which can react with NH_3 and H_2O to form $(NH_4)_2SO_4$ and NH_4HSO_4; the former dries powdery, which decomposes at 280 °C [14], but the latter is a kind of corrosive and sticky substance, which decomposes at 390 °C [15], Secondly, MnO_x or CuO may react with SO_2 to form stable sulfate species, which can cut off the redox cycle of the catalyst [16] and hinder the adsorption and activation of NO on the surface of the catalyst [17]. As such, the development of Mn-based catalysts with superior SO_2 resistance has attracted wide concern by many researchers.

The main method to improve SO_2 resistance is adding other modification metals/non-metals to SCR catalyst. Chang et al. [18] reported that the NO conversion over the SnO_x–MnO_2–CeO_2 catalyst exhibited 60% approximately in the presence of SO_2 and H_2O, which is much higher than that over MnO_2–CeO_2. The promotion effect is ascribed to the enhanced Lewis acid by the addition of SnO_x. Gao et al. [19] found that the Ni- or Co-doped MnO_2–CeO_2 catalyst exhibited higher SO_2 resistance owing to the formation of bidentate nitrate rather than monodentate nitrite species, which is less influenced by SO_2, inhibiting the formation of ammonium sulfate and metal sulfate species. Zhang et al. [20] investigated the promotion effect of F on SCR activity and SO_2 resistance over the CeO_2–MoO_2/TiO_2 catalyst. They concluded that the enhanced SCR performance is attributed to more generation of Oα species and promoted synergistic interaction among metal oxides by the doping of fluorine. Another method is to improve the preparation method of the Mn-based catalyst. Yao et al. [21] found that the MnO_2-based catalyst prepared by impregnation method in acetic acid solvent shows better SCR activity and SO_2 resistance than in deionized water, anhydrous ethanol, and oxalic acid, owing to the evenly dispersed MnO_x and enhanced interaction between metal oxides. Yu et al. [22] investigated the effect of Fe addition into Mn/TiO_2 catalyst via sol–gel and impregnation methods and they reported that the promotion of SO_2 resistance is related to the catalyst structure rather than the catalyst's components.

In the present work, the Cu–Mn/SAPO-34 zeolite catalysts were prepared by impregnation method. For promoting the SO_2 resistance over Cu–Mn/SAPO-34 catalyst, the proper modification metals with less affinity toward SO_2 and H_2O were filter by density functional theory (DFT) using Materials Studio 2016. The promotion effect of the transition metals-doped Cu–Mn/SAPO-34 catalyst on SCR activity and SO_2 resistance was further verified by the experimental study and comprehensive characterizations. It is expected that the present work will obtain more insights into improving the SO_2 resistance to low-temperature SCR reaction over the Cu–Mn/SAPO-34 catalyst.

2. Results and Discussion

2.1. Calculation of NH_3, NO, H_2O, or SO_2 Adsorption on Different Transition Metal Oxides

The adsorption of NH_3, NO, H_2O, and SO_2 on the surface of various metal oxides was calculated by Materials Studio 2016 using density functional theory. Firstly, the Fukui function was calculated to predict the active site (in Figure 1).

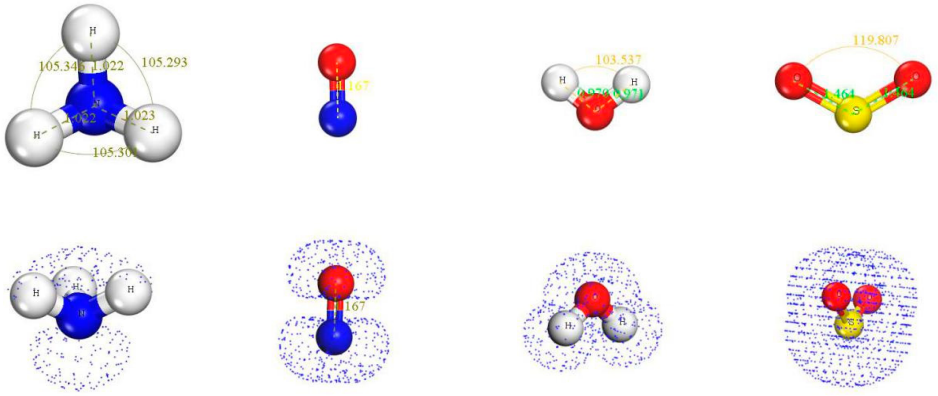

(**a**) NH_3 (**b**) NO (**c**) H_2O (**d**) SO_2

Figure 1. Structure and Fukui's function of several different gas molecules.

The adsorption energies, bond lengths, and angles of NH_3, NO, H_2O, and SO_2 on different transition metal oxides are shown in Table 1. It can be seen from the calculated results that the bond lengths of the adsorbed gas molecules have been changed. For the adsorption of NH_3 on CuO_x (001), the bond length was decreased from 1.037 Å to 1.022 Å, and the bond length of NO was increased from 1.167 Å to 1.224 Å after adsorption on MnO_x (001). The changed length of these bonds will lead to NH_3 and NO bonds that are easy to break and more lively to participate in SCR reaction, while the bond of H_2O and SO_2 will also be extended to be easy to break and to participate in the reaction, leading to the deactivation of SCR catalyst due to the SO_2 and H_2O poisoning. The results show that the bond lengths of NH_3 and NO molecules are relatively longer after adsorption on the oxides of Cu, Mn, Ce, and Co, and the bond lengths of H_2O and SO_2 are relatively small. In terms of adsorption energy, the adsorption capacity of different gas molecules on the same metal oxide adsorbed base is quite different. For example, the adsorption of NO on MnO_x is smaller than that of H_2O, which means that NO and H_2O compete on MnO_x and H_2O is more likely to adsorb on MnO_x. The adsorption energy of the gas molecules on different metal oxides is also different. For example, the adsorption energy of NH_3 on CuO_x is the highest, while it is the lowest on RuO_x, which means that NH_3 preferentially adsorb on CuO_x. In order to improve the H_2O resistance and SO_2 resistance properties of the catalyst, it is necessary to select proper transition metal oxides that easily adsorb NH_3 and NO, and do not easily adsorb H_2O and SO_2 as adjuvants. Based on the results calculated from Table 1, the Fe, Co, and Ce are beneficial for NH_3 and H_2O adsorption, while the adsorption of H_2O and SO_2 is less favorable on these metal oxides. Therefore, the Cu–Mn/SAPO-34 catalysts were further modified by these different metal oxides to improve the H_2O and SO_2 resistance properties.

Table 1. Adsorption structure and adsorption energy.

Adsorption Base	Adsorbents	Adsorption Energy/eV	Bond length/Å		Bond Angle/°	
			Before Adsorption	After Adsorption	Before Adsorption	After Adsorption
MnO_x(001)	NH_3	−2.03875	1.022 1.022 1.023	1.023 1.023 1.023	105.293 105.346 105.301	108.475 108.497 108.309
	NO	−1.05696	1.167	1.224	180	180
	H_2O	−1.10298	0.97 0.971	0.97 1	103.537	103.317
	SO_2	−2.20810	1.464 1.464	1.572 1.572	119.807	112.639

Table 1. *Cont.*

Adsorption Base	Adsorbents	Adsorption Energy/eV	Bond length/Å		Bond Angle/°	
			Before Adsorption	After Adsorption	Before Adsorption	After Adsorption
CuO_x(001)	NH_3	−3.52843	1.022	1.036	105.293	106.817
			1.022 1.023	1.036 1.037	105.346 105.301	106.817 106.742
	NO	−1.76270	1.167	1.201	180	180
	H_2O	−1.11959	0.97 0.971	0.988 0.979	103.537	106.312
	SO_2	−6.13501	1.464 1.464	1.614 1.614	119.807	107.336
CeO_x(001)	NH_3	−3.25139	1.022 1.022 1.023	1.034 1.034 1.034	105.293 105.346 105.301	107.880 107.872 107.791
	NO	−1.60770	1.167	1.205	180	180
	H_2O	−0.86146	0.97 0.971	0.991 0.991	103.537	105.937
	SO_2	−2.57682	1.464 1.464	1.558 1.557	119.807	112.783
FeO_x(001)	NH_3	−3.16140	1.022 1.022 1.023	1.033 1.033 1.033	105.293 105.346 105.301	108.603 108.636 108.564
	NO	−1.59895	1.167	1.20	180	180
	H_2O	−1.29654	0.97 0.971	0.987 1.030	103.537	104.996
	SO_2	−2.69020	1.464 1.464	1.554 1.555	119.807	113.179
CoO_x(001)	NH_3	−2.79458	1.022 1.022 1.023	1.033 1.034 1.034	105.293 105.346 105.301	108.971 109.051 108.835
	NO	−1.59260	1.167	1.208	180	180
	H_2O	−1.02839	0.97 0.971	0.993 0.994	103.537	104.911
	SO_2	−2.37824	1.464 1.464	1.629 1.630	119.807	113.453
MoO_x(001)	NH_3	−1.86400	1.022 1.022 1.023	1.028 1.028 1.029	105.293 105.346 105.301	110.208 110.182 110.251
	NO	−1.02833	1.167	1.180	180	180
	H_2O	−1.16968	0.97 0.971	0.987 0.987	103.537	105.752
	SO_2	−3.07422	1.464 1.464	1.540 1.540	119.807	113.453

Table 1. *Cont.*

Adsorption Base	Adsorbents	Adsorption Energy/eV	Bond length/Å		Bond Angle/°	
			Before Adsorption	After Adsorption	Before Adsorption	After Adsorption
$CrO_x(001)$	NH_3	−2.75508	1.022 1.022 1.023	1.027 1.028 1.029	105.293 105.346 105.301	107.530 107.433 107.470
	NO	−1.49119	1.167	1.206	180	180
	H_2O	−1.12858	0.97 0.971	0.995 0.995	103.537	106.029
	SO_2	−3.22779	1.464 1.464	1.559 1.560	119.807	113.015
$RuO_x(001)$	NH_3	−1.11775	1.022 1.022 1.023	1.032 1.031 1.032	105.293 105.346 105.301	109.292 109.044 109.714
	NO	−0.87561	1.167	1.200	180	180
	H_2O	−0.10325	0.97 0.971	0.971 0.970	103.537	103.537
	SO_2	−2.65537	1.464 1.464	1.549 1.553	119.807	112.669

2.2. Changes of Catalyst Activity after Adding Transition Metals

Figure 2 illustrates the changes of Cu–Mn/SAPO-34 catalyst activity after adding transition metals. It can be seen from Figure 2 that the Cu–Mn/SAPO-34 exhibits superior low-temperature SCR activity, which is up to 79% and 88% at 150 °C and 180 °C, respectively. The addition of transition metals has a significant promoting effect on the low-temperature SCR activity of the Cu–Mn/SAPO-34 catalyst, especially by the addition of Ce and Co. However, with the increase of reaction temperature to 270 °C, the activity of partially modified catalysts is lower than the Cu–Mn/SAPO-34 catalyst. Moreover, the activity of the Co- and Fe-modified Cu–Mn/SAPO-34 catalysts are decreased compared with that at 240 °C. This result demonstrates that the addition of transition metals enhance the oxidation ability of the catalyst, causing the catalytic oxidation of NH3 to NO (i.e., C–O reaction) at higher temperatures [23,24]. Among all three transition metals, the Ce-modified Cu–Mn/SAPO-34 exhibits the highest SCR activity in the wide temperature range between 90 °C and 330 °C.

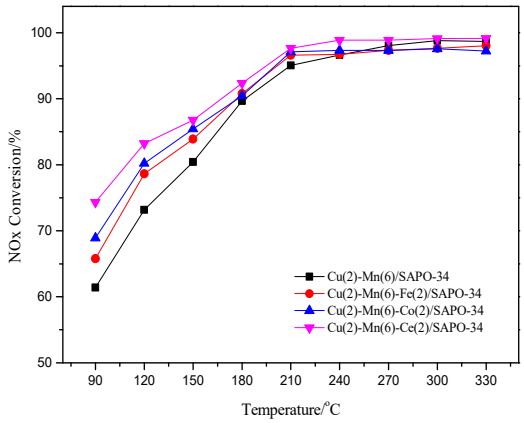

Figure 2. Changes of denitrification activity of Cu–Mn/SAPO-34 catalyst after modification of different transition metal additives. Reaction conditions: 350 ppm NO, 350 ppm NH_3, 3% O_2, N_2 balance, 500 ppm SO_2 (when used), and GHSV = 15,000 h^{-1}.

2.3. Changes of SO_2 Resistance Performance of Catalyst after Adding Different Transition Metal Additive

Figure 3 shows the changes of SO_2 resistance performance of Cu–Mn/SAPO-34 catalyst after modification of different transition metal additives. For the Cu–Mn/SAPO-34 catalyst, the SCR activity declines immediately with the injection of SO_2 into the gas atmosphere. NO_x conversion of Cu–Mn/SAPO-34 catalyst decreases from 96.6% to 67% in the presence of 500 ppm SO_2 for 8 h at 240 °C, indicating the severe poisoning effect of SO_2 over the Cu–Mn/SAPO-34 catalyst. With the modification of transition metal additives, the Cu–Mn–Fe/SAPO-34, Cu–Mn–Co/SAPO-34, and Cu–Mn–Ce/SAPO-34 could still provide about 75%, 82%, and 85%, respectively, after the injection of SO_2 for 8 h under the same condition. Based on this result, it can be seen that the addition of Fe, Co, or Ce can all enhance SO_2 resistance of the Cu–Mn/SAPO-34 catalyst significantly. Among them, the modification of Ce shows the best SO_2 resistance performance, which is consistent with the results of Wu [25], Jin [26], and Liu et al. [27]. This result demonstrates that the modification of Ce on Cu–Mn/SAPO-34 promotes both the SCR activity and the SO_2 resistance performance.

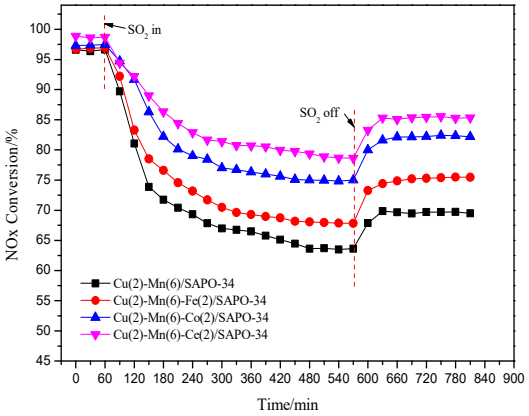

Figure 3. Changes of anti-SO_2 performance of Cu–Mn/SAPO-34 catalyst after modification of different transition metal additives.

2.4. Catalyst Characterization

2.4.1. BET Analysis

The specific surface area, pore volume, and pore size of fresh and SO_2-poisoned catalysts are determined by N_2 adsorption and are summarized in Table 2. As shown in Table 2, the specific surface area and pore volume of the catalyst after the addition of the additive decreased, while the pore size increased. This may be due to the additive covered in the catalyst surface or into the molecular sieve channel. Among all the modified Cu–Mn/SAPO-34 catalysts, the addition of Ce exhibited the highest surface area, which may promote the adsorption of NH3 and NO, facilitating the SCR reaction as shown in Figure 2. After SO_2 poisoning for 8 h, the surface area and the pore volume of all the catalysts decreased and the pore diameters extended. These results suggest that sulfate species deposit on the surface of the Cu–Mn/SAPO-34 catalyst and mesopores are blocked from forming micro pores after SO_2 poisoning. From a comparison of the relative reduction of surface area before and after poisoning, it can be seen that the surface area of modified catalysts decreased in the order of Fe-modified (18.6%) > Co-modified (11.1%) > Ce-modified (7.8%). The decrease of the BET surface area of the catalyst after SO_2 poisoning is mainly due to the deposition of ammonium sulfate and metal sulfites/sulfates according to the thermal gravity analysis (TG) and XRD analysis (Figures 5 and 6), which lowered the SCR activity of the modified Cu–Mn/SAPO-34 catalyst. However, the addition of Ce into the Cu–Mn/SAPO-34 catalyst maintained a relatively large specific surface area and, thus, retained the highest SO_2 resistance ability in the SCR reaction.

Table 2. BET analysis of the fresh and spent Cu–Mn/SAPO-34 or modified catalyst.

Catalyst	BET Surface Area (m^2/g)	Pore Volume (cm^3/g)	Pore Diameter (nm)	BET Relative Reduction (%)
Fresh catalyst	457	0.23	2.08	27.4
Used catalyst	332	0.16	2.15	
Fe-modified catalyst (Fresh)	399	0.21	2.03	18.6
Fe-modified catalyst (Used)	325	0.14	3.34	
Co-modified catalyst (Fresh)	402	0.17	2.22	11.1
Co-modified catalyst (Used)	357	0.15	2.35	
Ce-modified catalyst (Fresh)	423	0.19	2.14	7.8
Ce-modified catalyst (Used)	390	0.16	2.18	

2.4.2. Temperature Programmed Desorption of Ammonia (NH_3-TPD) Analysis

Another crucial property for the SCR reaction is the surface acidity of the catalysts. NH_3-TPD experiment was performed to characterize the acidity of the catalysts before and after SO_2 poisoning (Figure 4). It can be seen from Figure 4 that the surface acidity of the modified Cu–Mn/SAPO-34 catalysts are slightly increased, as can be deduced by the comparison between the peak areas of the modified and the original Cu–Mn/SAPO-34 catalyst, which may be due to the increase of the number of acid sites on the surface of the catalyst. The relative acidity of the original and modified Cu–Mn/SAPO-34 catalysts after SO_2 poisoning was reduced, and the reductions were in the order of Fe-modified > Co-modified > Ce-modified, which is consistent with the order of the reduction of surface area as shown in Table 2. The slightly decreased acidity over the SO_2-poisoned Co-modified and Ce-modified Cu–Mn/SAPO-34 catalysts maintain the adsorption amounts of NH_3, facilitating the proceeding of the SCR reaction. The insight into the different behavior of surface acidity over Fe-, Co-, and Ce-modified Cu–Mn/SAPO-34 catalysts after SO_2 poisoning will be further discussed.

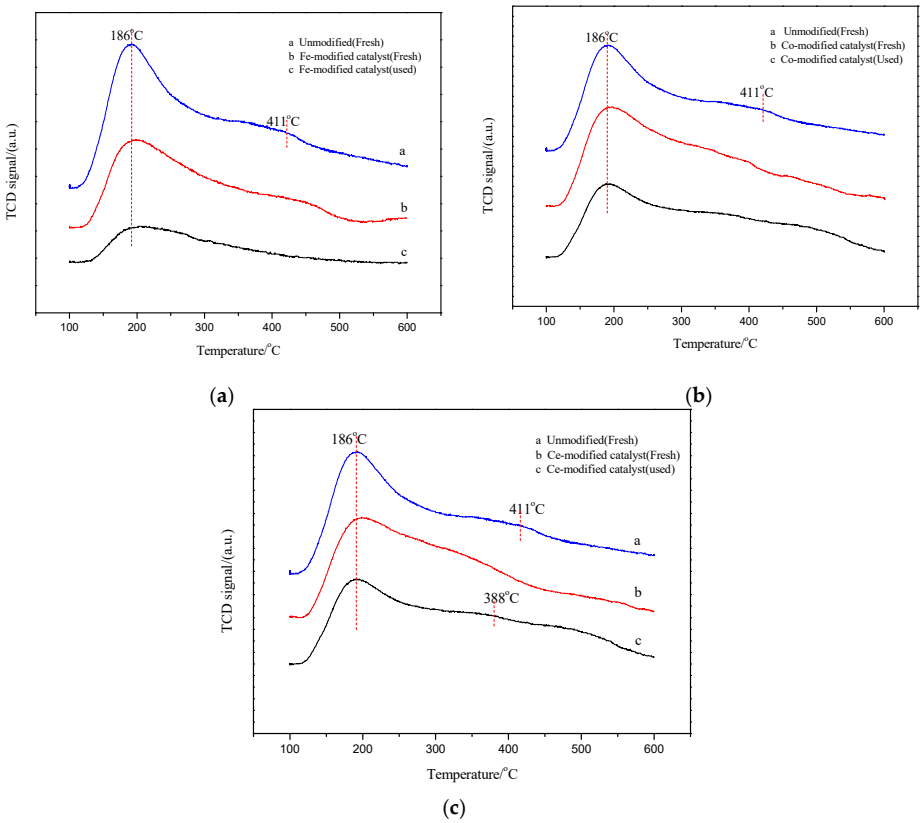

Figure 4. NH_3-TPD diagram of SO_2 poisoning catalyst before addition of different transition metal additives ((**a**) Fe, (**b**) Co, (**c**) Ce).

2.4.3. TG-differential thermal gravity (DTG) Analysis

The catalysts after SO_2 poisoning were characterized by TG-DTG to determine the sulfate species and relative contents of different S-containing species. As shown in Figure 5, all the TG curves presented three major weight losses, and the first one appeared at about 100 °C, which was due to the evaporation of water in the sample [28]. The second one emerged at 200~400 °C, which was close to the decomposition temperatures of $(NH_4)_2SO_4$ (230 °C) and NH_4HSO_4 (350 °C), as reported in the literature [29,30]. The third loss above 700 °C could be ascribed to the thermal decomposition of the active component sulfites/sulfates. For the Cu–Mn/SAPO-34 catalyst, an obvious weight loss centered at 356 °C was observed, which can be attributed to the decomposition of $(NH_4)_2SO_4$. A faint weight loss centered at 821 °C was also observed according to the TG spectra, which can be assigned to the decomposition of metal sulfates on the surface of the catalyst. This result demonstrates that the main reason for the deactivation of Cu–Mn/SAPO-34 catalyst is the deposition of a good amount of $(NH_4)_2SO_4$, depositing on the pore channel and inhibiting the adsorption of the NH_3 and NO [22]. After the modification of Fe, Co, and Ce, the decomposition peak attributed to $(NH_4)SO_4$ and NH_4HSO_4 was lower than that of Cu–Mn/SAPO-34 catalyst, indicating that the decomposition of ammonium sulfates was accelerated. Moreover, the weight loss attributed to the decomposition of $(NH_4)SO_4$ and NH_4HSO_4 over the Ce-modified Cu–Mn/SAPO-34 was the smallest among all the modified catalyst.

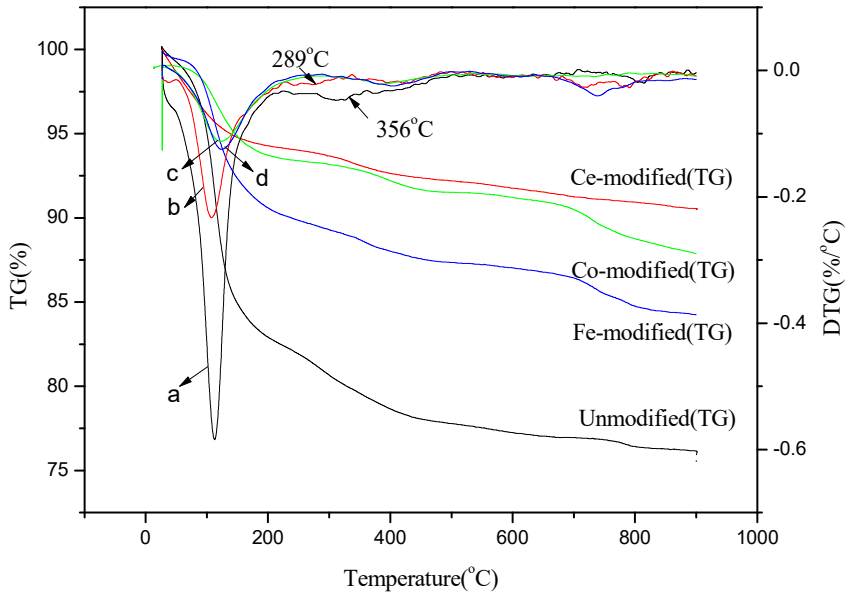

Figure 5. Thermal gravity analysis (TG)-differential thermal gravity (DTG) diagram of catalyst SO_2 poisoning after addition of different transition metal additives (**a**: Unmodified, **b**: Ce-modified, **c**: Co-modified, **d**: Fe-modified).

As for the Fe-modified Cu–Mn/SAPO-34 catalyst, the decomposition peak centered at 751 °C was strengthened compared to that of the Cu–Mn/SAPO-34 catalyst. It is reasonable to speculate that the decomposition peak is attributed to the decomposition of $FeSO_4$ or $Fe_2(SO_4)_3$ [31]. With the modification of Ce, the weight loss ascribed to the decomposition of metal sulfates is reduced according to the TG spectra, while the decomposition peaks centered at 743 °C is still observed, indicating that the modification of Ce prevents the sulfation of MnO_2 or CuO_2. Therefore, it can be explained that the main reason for the deactivation of the catalyst by SO_2 poisoning at 240 °C after Ce modification is the formation of ammonium sulfate on the surface of the catalyst. Most of the ammonium sulfate can be decomposed, indicating that the catalyst can be regenerated by heat treatment. Moreover, as illustrated in Figure 5, in the case of the Cu(2)–Mn(6)–Ce(2)/SAPO-34 catalyst, the decomposition peak attributed to NH_4HSO_4 appeared at a much lower temperature (at approximately 289 °C) than that on the Cu(2)–Mn(6)/SAPO-34 catalyst. This finding indicated that the thermal stability of

NH_4HSO_4 on the Cu(2)–Mn(6)–Ce(2)/SAPO-34 catalyst was greatly reduced compared to that of the Cu(2)–Mn(6)/SAPO-34 catalyst.

2.4.4. XRD Analysis

Figure 6 Shows the XRD spectra of Cu–Mn/SAPO-34 and Ce-modified Cu–Mn/SAPO-34 catalysts before and after SO_2 poisoning. After the SO_2 poisoning process, several new diffraction peaks were observed at 11.93°, 21.08°, 31.46°, and 33.11° for Cu–Mn/SAPO-34 catalyst, and the anterior two peaks were due to the formation of NH_4HSO_4(PDF#25-0034), $CuSO_4$(PDF28-0401), and the latter two were assigned to $(NH_4)_2SO_4$(PDF#40-0660) and $MnSO_4$(PDF35-0751). With the introduction of Ce to the Cu–Mn/SAPO-34 catalyst, the peak attributed to $Ce(SO_4)_2$ appeared, while no peak ascribed to $MnSO_4$ and $(NH_4)_2SO_4$ was observed. It is possible that the addition of Ce reduces the accumulation of ammonium sulfate on the surface of the catalyst, and the sulfation of Ce effectively protects the active component Mn from being sulfated, resulting in a significant increase in the resistance to SO_2 with the addition of Ce promoter.

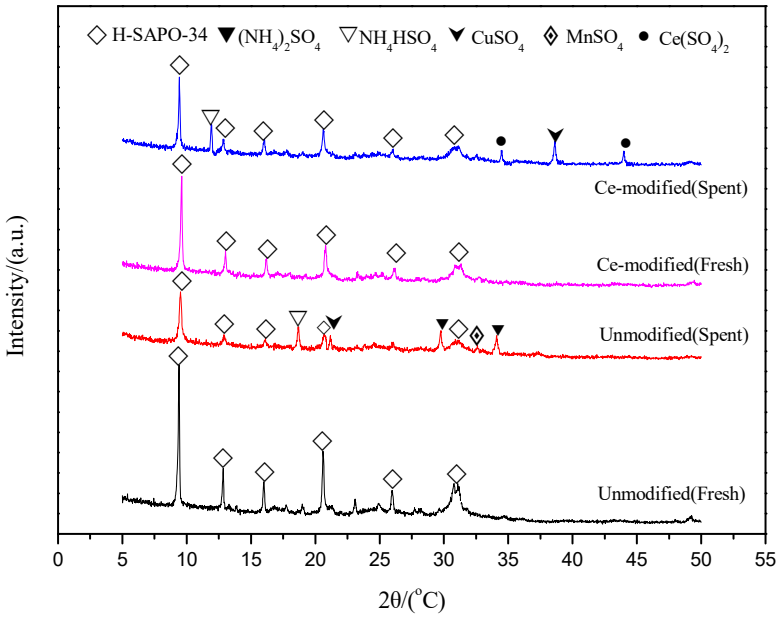

Figure 6. XRD pattern of 2% Ce-modified catalyst after SO_2 poisoning.

2.4.5. SEM and EDX Analysis

In order to observe the changes of the surface morphology and the amount of the surface elements of the modified catalyst before and after SO_2 poisoning, SEM and EDX experiments were conducted and the results are shown in Figure 7 and Table 3. As illustrated in Figure 7, the surface of fresh catalysts were smooth and uniform (Figure 7a). After 500 ppm SO_2 poisoning for 8 h, a significant agglomeration and sulfates deposited on the surface could be observed in the Figure 7b. Combined with EDS, XRD and TG-DTG results, it is reasonable to speculate that this can be attributed to the deposition of a good amount of ammonium sulfate salts as shown in Figure 7b. While with the modification of Ce, Co, or Fe, only a few deposited particles and agglomeration could be seen in the Figure 7c–e. The content of S element on the surface of the Ce-modified catalyst after SO_2 poisoning was significantly lower than that of other catalysts, indicating that the catalyst modified by Ce could reduce the deposition of ammonium sulfate on the surface of the catalyst. The research of Jin et al. [26] indicated that Ce can reduce the bond energy between NH_4^+ and SO_4^{-2} or HSO_4^{-1}, reducing the thermal stability of $(NH_4)_2SO_4$ and NH_4HSO_4, which may result in the easier decomposition of ammonium sulfates, thereby reducing the accumulation of ammonium sulfate on the catalyst surface.

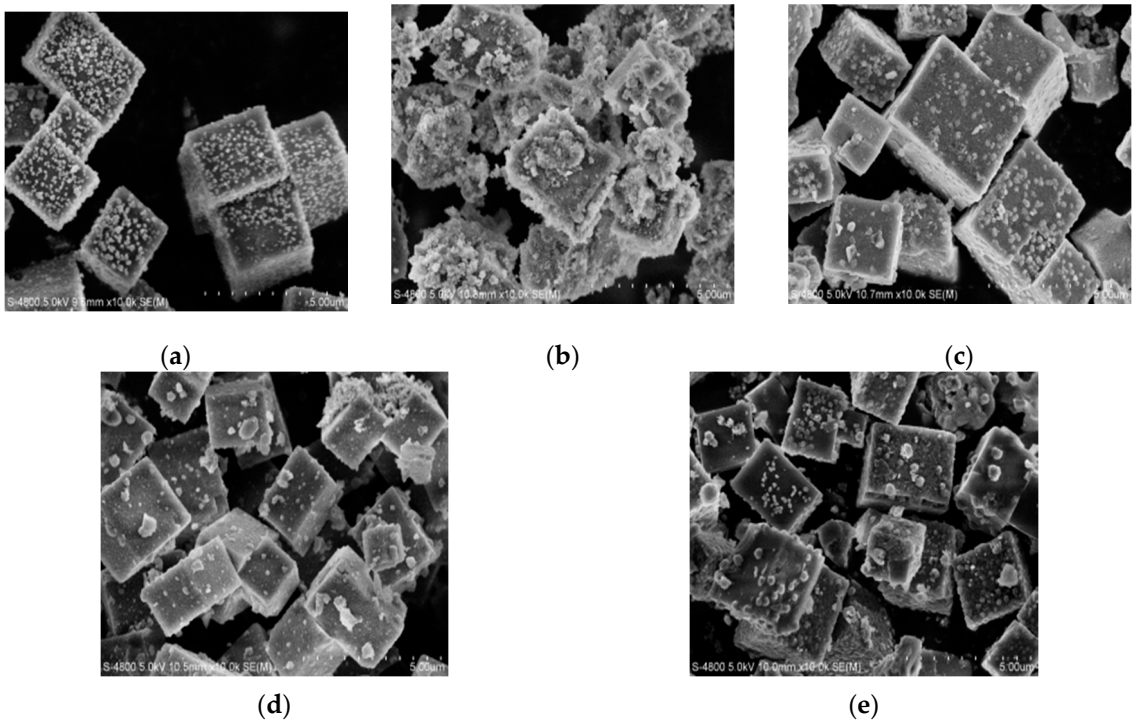

Figure 7. SEM images of several different catalysts. (**a**) fresh Cu-Mn/SAPO-34; (**b**) SO_2-poisoned Cu-Mn/SAPO-34; (**c**) SO_2-poisoned Ce-Cu-Mn/SAPO-34; (**d**) SO_2-poisoned Co-Cu-Mn/SAPO-34; (**e**) Fe-Cu-Mn/SAPO-34.

Table 3. Surface elements of several different catalysts.

	O	Si	Al	P	Cu	Mn	Ce	Co	Fe	S
Unmodified (Fresh)	62.57	3.51	16.47	13.98	1.11	2.36	–	–	–	–
Unmodified (Spent)	59.54	3.19	16.42	14.76	1.24	3.37	–	–	–	1.48
Ce-modified (Spent)	57.09	4.33	19.74	10.62	1.46	4.52	1.89	–	–	0.35
Co-modified (Spent)	55.63	4.71	18.77	12.31	1.28	4.82	–	1.84	–	0.64
Fe-modified (Spent)	55.94	4.13	16.32	14.49	1.45	4.63	–	–	1.91	1.13

Based on the SCR activity tests in the presence of SO_2 and characterizations, it can be concluded that the Cu–Mn/SAPO-34 catalyst, after SO_2 poisoning for 8 h, is deposited by ammonium sulfates and metal sulfates such as $MnSO_4$ and $CuSO_4$ according to the TG-DTG and XRD analysis. However, the formation of $MnSO_4$ and $CuSO_4$ is not the main reason for the deactivation of the Cu–Mn/SAPO-34 by SO2 poisoning due to the limited formation of metal sulfates shown in TG-DTG analysis. The good amount of ammonium sulfates deposited on the active sites reduce the surface area, inhibiting the adsorption of NH_3 as shown in Figure 4a, and deactivating the Cu–Mn/SAPO-34 catalyst. Meanwhile, for the modified Cu–Mn/SAPO-34 catalyst by Fe, Co, and Ce oxides, the SO_2 resistance performance is enhanced significantly owing to less deposition of ammonium sulfates, which can be observed intuitively by the SEM-EDX analysis. It can be concluded that the modification of Fe, Co, and Ce oxides facilitate the decomposition of NH_4HSO_4. Among all the modified Cu–Mn/SAPO-34 catalysts, the Ce-modified Cu–Mn/SAPO-34 exhibited the highest SO_2 resistance performance. According to the previous study, the ceria has been found to be highly reactive in the SCR reaction due to the high oxygen-storage capacity (OSC) and the excellent redox ability by the reversible transition between Ce^{4+} and Ce^{3+} [32]. Thus, the Ce-modified Cu–Mn/SAPO-34 exhibited the highest SCR activity among all the modified Cu–Mn/SAPO-34 catalysts. Combining with the XRD results, it can be speculated that the ceria component in the Cu–Mn-Ce/SAPO-34 catalyst acts as a trapper for capturing SO_2 to form $Ce(SO_4)_2$, which inhibits the deposition of ammonium sulfates due to the consumption of SO_2 [33].

Moreover, the addition of Ce oxides decreases thermal stability of ammonium sulfates by lowering the decomposition temperature of ammonium sulfates as shown in TG-DTG analysis [25].

3. Experimental

3.1. Catalyst Preparation

The molecular sieve was modified by impregnation method. A certain amount of zeolite molecular sieve H-SAPO-34 (n(P_2O_5):n(SiO_2):n(Al_2O_3) = 1:1:1), provided by Nankai university, was weighed and dried in a drying oven at 105 °C for 30 min. A certain amount of $Cu(NO_3)_2{\cdot}3H_2O$ powder was mixed with manganese nitrate solution with the mass fraction of 50% in the beaker of 200 mL, and then 50 mL of deionized water was added into the immersion liquid. A certain amount of iron nitrate, cobalt nitrate, or cerium nitrate was added during the mixing process for preparing Fe-, Co-, or Ce-modified Cu–Mn/SAPO-34. Then, the beaker with a magnetic stirrer inside was immersed in a water bath at the constant temperature of 40 °C. After 12 h of immersion, the solution was thoroughly mixed and heated until the moisture was completely evaporated. The powder was then put into a dry oven at about 100 °C for 12 h. The dried power was grinded and sieved by the 40 to 60 mesh. The obtained powders were placed in a tube furnace and calcined at 450 °C for 6 h to obtain the catalyst sample for the experiment. The catalyst sample Cu(2)–Mn(6)/SAPO-34(450) indicated that the mass fraction of 2% Cu and 6% Mn were loaded on the molecular sieve SAPO-34 with the calcination temperature of 450 °C.

3.2. Catalytic Activity Measurement

Denifitrication activity measurements using NH_3 were carried out in a fixed-bed stainless-steel tubular flow reactor (inner diameter: 16 mm) (Figure 8). The tube furnace of the reactor can be heated from the room temperature to 800 °C. The gas feeding system was composed of five gas feeding pipes controlled by the mass flow meter (0~1.5 L) and one liquid feeder micro injection pump (0.001 μL/min~127 mL/min), equipped with the reactor for adjusting the composition of the feeding gas. The reaction temperature in the experiments was set to be changed from 90 to 330 °C. Then, 2 mL catalyst was placed on the holder of the reactor, and the feeding gas consisted of 350 ppm NO, 350 ppm NH_3, 3 vol % O_2 and N_2 as the balance. Further, 500~1500 ppm SO_2 was injected into the feeding gas for investigating the effect of SO_2 on the catalyst poisoning. The GHSV was set to be 15,000 h^{-1}. The gas composition of the reactor inlet and outlet was collected by an air bag and analyzed by the flue gas analyzer (Testo 350). The NO conversion was obtained from the equation as follows:

$$\eta = \frac{C_{NO}^{in} - C_{NO}^{out}}{C_{NO}^{in}} \times 100\% \quad (1)$$

where η, C_{NO}^{in}, and C_{NO}^{out} represent the NO conversion, inlet, and outlet NO concentration.

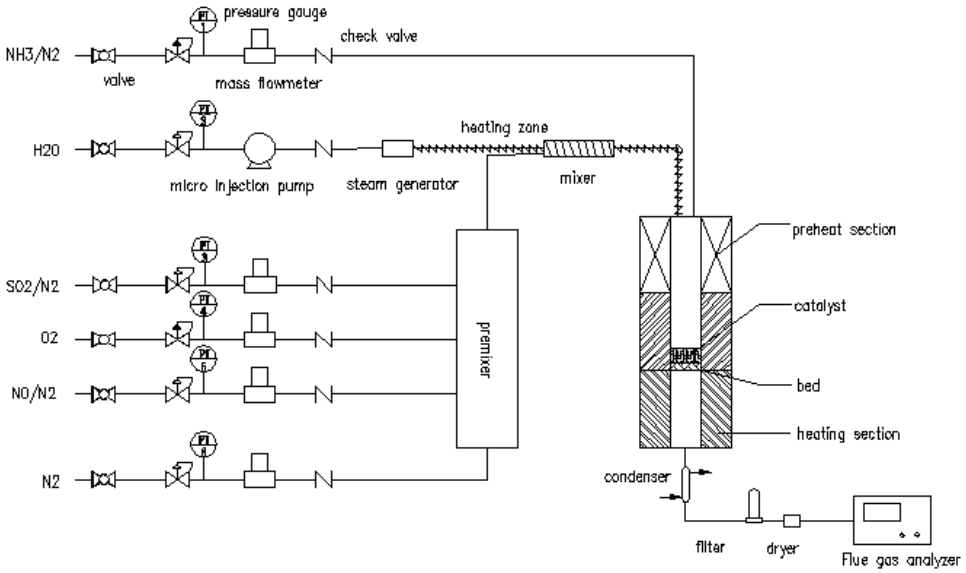

Figure 8. Schematics for the fixed-bed tubular flow reactor.

3.3. Catalyst Characterization

A Micromeritics ASAP 2010 M micropore size analyzer was used to measure the N_2 adsorption isotherms of the samples at liquid N_2 temperature (−196 °C). Specific surface area, pore volume, and pore diameter were determined by N_2 adsorption using the BET and Barrett-Joyner-Halenda (BJH) methods.

The XRD measurements were carried out on a Rigaku D/Smartlab (III) system with Cu Ka radiation. The X-ray source was operated at 40 kV and 40 mA. The diffraction patterns were taken in the 2θ range of 5~50° at a scan speed of 10° min^{-1} and a resolution of 0.02°. The bulk atomic concentrations were determined by X-ray energy dispersive spectroscopy (EDS) linked with scanning electron microscopy (SEM) in SIRON-50 system at a voltage of 150 eV. Thermal gravity analysis (TG) and differential thermal gravity (DTG) were performed using the Nanjing exhibition electrical and mechanical technology company produced TGA-101 type, with the instrument accuracy of 0.2 μg, heating rate of 15 °C min^{-1} in a flowing of N_2; the temperature rose from room temperature to 900 °C.

Temperature programmed desorption of ammonia (NH_3-TPD) was carried out on an FINESORB-3010 instrument provided by Zhejiang Pantech Instrument Company. Approximately 0.05 g of powder catalyst was firstly pretreated in a stream of He at 20 mL/min while heating up to 300 °C. After a hold time of 30 min, the sample was cooled down to 100 °C and saturated with a 20 mL/min gas mixture of 5% NH_3 in He for 30 min. At the end of the saturation process, the sample was flushed with pure He at 50 mL/min until the TCD signal was stabilized. The sample was then heated up to 600 °C (ramp 10 °C/min) and the mass spectrum signal of NH_3 desorbed from the catalyst surface was collected.

3.4. Calculation Details

All calculations are based on DFT, and are performed using Materials Studio 2016 modeling $DMol^3$. Double-numerical quality basis set with polarization function (DNP) and GGA-PBE was used. The real space cutoff radius is maintained as 4.7Å. The Brillouin zone is sampled using a (1 × 2 × 1) Monkhorst-Pack grid, which ensures the convergence of the entire system.

The binding energies (E_{ad}) of the NH_3, NO, H_2O, or SO_2 molecule are calculated for all possible active acid sites on the surfaces as follows:

$$E_{ad} = E_{adsorbed-substrate} - (E_{adsorbed} + E_{substrate}) \quad (2)$$

where $E_{adsorbed\text{-}substrate}$ is the energy of the structure after adsorption, $E_{adsorbed}$ is the energy of the adsorbent, and $E_{substate}$ is the energy of the adsorbed base. Note that a positive value for E_{ad} suggests stable adsorption, which means that the adsorbent is more easily adsorbed.

4. Conclusions

The SCR activity of Cu–Mn/SAPO-34 catalyst modified by Fe, Co, and Ce oxides in the absence/presence were tested. Significantly enhanced low-temperature SCR activity and SO_2 resistance were found. Comprehensive characterizations including BET, XRD, TG-DTG, SEM, and EDX were carried out to investigate the mechanism of the promoting effect of the modification. It can be concluded that the deactivation of Cu–Mn/SAPO-34 is attributed to the deposition of a good amount of ammonium sulfates, depositing on the active sites and inhibiting the adsorption of NH_3. With the modification of Fe, Co, and Ce oxides, the SO_2 resistance performance is enhanced significantly owing to less deposition of ammonium sulfates. The decomposition of ammonium sulfates was facilitated by the modification of Fe, Co, and Ce oxides, which can be observed intuitively by the SEM-EDX analysis. Among all the modified Cu–Mn/SAPO-34 catalysts, the Ce-modified Cu–Mn/SAPO-34 exhibited the highest SO_2 resistance performance, owing to less formation of ammonium sulfates, as the ceria acted as a trapper for the capturing SO_2 to form $Ce(SO_4)_2$. Moreover, the addition of ceria decreased decomposition temperature of ammonium sulfates, further inhibiting the deposition to ammonium sulfates.

Author Contributions: Funding acquisition, D.S.; Investigation, G.L., W.Z., P.H. and C.G.; Methodology, G.L., W.Z., P.H. and C.W.; Supervision, D.S. and C.W.; Writing—original draft, G.L., W.Z. and P.H.; Writing—review & editing, G.L., W.Z. and D.S.

Funding: This work was supported by National Natural Science Foundation of China [Grant no. 51676047 and 5181101221], the international collaboration project from Department of Science and Technology of Jiangsu Province [grant number BZ2017014], Key Project of Environmental Protection Research Program of Department of Ecology and Environment of Jiangsu Province [grant number 2017006], Nanjing Science and Technology Planning Project of Nanjing Science and Technology Committee of Jiangsu Province [grant number 201716003].

Conflicts of Interest: The authors declare no conflict of interest.

References

1. Huang, Z.; Zhu, Z.; Liu, Z.; Liu, Q. Formation and reaction of ammonium sulfate salts on V2O5/AC catalyst during selective catalytic reduction of nitric oxide by ammonia at low temperatures. *J. Catal.* **2003**, *214*, 213–219. [CrossRef]
2. Busca, G.; Lietti, L.; Ramis, G.; Berti, F. Chemical and mechanistic aspects of the selective catalytic reduction of NOx by ammonia over oxide catalysts: A review. *Appl. Catal. B* **1998**, *18*, 1–36. [CrossRef]
3. Dunn, J.P.; Stenger, H.G., Jr.; Wachs, I.E. Oxidation of SO_2 over Supported Metal Oxide Catalysts. *J. Catal.* **1999**, *181*, 233–243. [CrossRef]
4. Huang, J.; Tong, Z.; Huang, Y. Selective catalytic reduction of NO with NH3 at low temperatures over iron and manganese oxides supported on mesoporous silica. *Appl. Catal. B Environ.* **2008**, *78*, 309–314. [CrossRef]
5. Du, X.S.; Gao, X.; Cui, L.W.; Fu, Y.C.; Luo, Z.Y.; Cen, K.F. Investigation of the effect of Cu addition on the SO2-resistance of a CeTi oxide catalyst for selective catalytic reduction of NO with NH_3. *Fuel* **2012**, *92*, 49–55. [CrossRef]
6. Liu, F.; He, H. Structure−Activity Relationship of Iron Titanate Catalysts in the Selective Catalytic Reduction of NO_x with NH_3. *J. Phys. Chem. C* **2010**, *114*, 16929–16936. [CrossRef]
7. Hu, H.; Cai, S.; Li, H.; Huang, L.; Shi, L.; Zhang, D. Mechanistic Aspects of deNO x Processing over TiO_2 Supported Co–Mn Oxide Catalysts: Structure–Activity Relationships and In Situ DRIFTs Analysis. *ACS Catal.* **2015**, *5*, 6069–6077. [CrossRef]
8. Zhang, S.; Li, H.; Zhong, Q. Promotional effect of F-doped V_2O_5–WO_3/TiO_2 catalyst for NH_3-SCR of NO at low-temperature. *Appl. Catal. A* **2012**, *435*, 156–162. [CrossRef]
9. Wallin, M.; Forser, S.; Thormählen, P.; Skoglundh, M. Screening of TiO_2-supported catalysts for selective NOx reduction with ammonia. *Ind. Eng. Chem. Res.* **2004**, *43*, 7723–7731. [CrossRef]

10. Kantcheva, M. FT-IR spectroscopic investigation of the reactivity of NOx species adsorbed on Cu^{2+}/ZrO_2 and $CuSO_4/ZrO_2$ catalysts toward decane. *Appl. Catal. B* **2003**, *42*, 89–109. [CrossRef]
11. Ma, L.; Cheng, Y.; Cavataio, G.; McCabe, R.W.; Fu, L.; Li, J. Characterization of commercial Cu-SSZ-13 and Cu-SAPO-34 catalysts with hydrothermal treatment for NH_3-SCR of NOx in diesel exhaust. *Chem. Eng. J.* **2013**, *225*, 323–330. [CrossRef]
12. Fan, Y.; Ling, W.; Huang, B.; Dong, L.; Yu, C.; Xi, H. The synergistic effects of cerium presence in the framework and the surface resistance to SO_2 and H_2O in NH_3-SCR. *J. Ind. Eng. Chem.* **2017**, *56*, 108–119. [CrossRef]
13. Liu, G.; Zhang, W.; He, P.; Guan., S.; Yuan, B.; Li, R.; Shen, D. H_2O and/or SO_2 Tolerance of Cu-Mn/SAPO-34 Catalyst for NO Reduction with NH_3 at Low Temperature. *Catalysts* **2019**, *9*, 289. [CrossRef]
14. Kiyoura, R.; Urano, K. Mechanism, kinetics, and equilibrium of thermal decomposition of ammonium sulfate. *Ind. Eng. Chem. Process Des. Dev.* **1970**, *9*, 489–494. [CrossRef]
15. Zhu, Z.; Niu, H.; Liu, Z.; Liu, S. Decomposition and reactivity of NH_4HSO_4 on V_2O_5/AC catalysts used for NO reduction with ammonia. *J. Catal.* **2000**, *195*, 268–278. [CrossRef]
16. Wijayanti, K.; Andonova, S.; Kumar, A.; Li, J.; Kamasamudram, K.; Currier, N.W.; Yezerets, A.; Olsson, L. Impact of sulfur oxide on NH_3-SCR over Cu-SAPO-34. *Appl. Catal. B Environ.* **2015**, *166*, 568–579. [CrossRef]
17. Jiang, B.Q.; Wu, Z.B.; Liu, Y.; Lee, S.C.; Ho, W.K. DRIFT study of the SO_2 effect on low-temperature SCR reaction over Fe– Mn/TiO_2. *J. Phys. Chem. C* **2010**, *114*, 4961–4965. [CrossRef]
18. Chang, H.; Li, J.; Chen, X.; Ma, L.; Yang, S.; Schwank, J.W.; Hao, J. Effect of Sn on MnO_x–CeO_2 catalyst for SCR of NO_x by ammonia: Enhancement of activity and remarkable resistance to SO_2. *Catal. Commun.* **2012**, *27*, 54–57. [CrossRef]
19. Gao, F.; Tang, X.; Yi, H.; Li, J.; Zhao, S.; Wang, J.; Chu, C.; Li, C. Promotional mechanisms of activity and SO_2 tolerance of Co-or Ni-doped MnO_x-CeO_2 catalysts for SCR of NO_x with NH_3 at low temperature. *Chem. Eng. J.* **2017**, *317*, 20–31. [CrossRef]
20. Zhang, G.; Huang, X.; Yang, X.; Tang, Z. Comprehensive study of the promotional mechanism of F on Ce–Mo/TiO 2 catalysts for wide temperature NH 3-SCR performance: the activation of surface [triple bond, length as m-dash] Ti–F bonds. *Catal. Sci. Technol.* **2019**, *9*, 2231–2244. [CrossRef]
21. Yao, X.; Kong, T.; Chen, L.; Ding, S.; Yang, F.; Dong, L. Enhanced low-temperature NH3-SCR performance of MnOx/CeO2 catalysts by optimal solvent effect. *Appl. Surf. Sci.* **2017**, *420*, 407–415. [CrossRef]
22. Yu, J.; Guo, F.; Wang, Y.; Zhu, J.; Liu, Y.; Su, F.; Gao, S.; Xu, G. Sulfur poisoning resistant mesoporous Mn-base catalyst for low-temperature SCR of NO with NH_3. *Appl. Catal. B Environ.* **2010**, *95*, 160–168. [CrossRef]
23. Xiong, S.; Xiao, X.; Liao, Y.; Dang, H.; Shan, W.; Yang, S. Global kinetic study of NO reduction by NH_3 over V_2O_5–WO_3/TiO_2: Relationship between the SCR performance and the key factors. *Ind. Eng. Chem. Res.* **2015**, *54*, 11011–11023. [CrossRef]
24. Yang, S.; Guo, Y.; Chang, H.; Ma, L.; Peng, Y.; Qu, Z.; Yan, N.; Wang, C.; Li, J. Novel effect of SO_2 on the SCR reaction over CeO_2: Mechanism and significance. *Appl. Catal. B Environ.* **2013**, *136*, 19–28. [CrossRef]
25. Wu, Z.; Jin, R.; Wang, H.; Liu, Y. Effect of ceria doping on SO_2 resistance of Mn/TiO_2 for selective catalytic reduction of NO with NH_3 at low temperature. *Catal. Commun.* **2009**, *10*, 935–939. [CrossRef]
26. Jin, R.; Liu, Y.; Wang, Y.; Cen, W.; Wu, Z.; Wang, H.; Weng, X. The role of cerium in the improved SO_2 tolerance for NO reduction with NH_3 over Mn-Ce/TiO_2 catalyst at low temperature. *Appl. Catal. B* **2014**, *148*, 582–588. [CrossRef]
27. Jin, R.; Liu, Y.; Wu, Z.; Wang, H.; Gu, T. Relationship between SO_2 poisoning effects and reaction temperature for selective catalytic reduction of NO over Mn–Ce/TiO_2 catalyst. *Catal. Today* **2010**, *153*, 84–89. [CrossRef]
28. Zhang, B.; Chen, B.; Shi, K.; He, S.; Liu, X.; Du, Z.; Yang, K. Preparation and characterization of nanocrystal grain TiO_2 porous microspheres. *Appl. Catal. B* **2003**, *40*, 253–258.
29. Shi, Y.J.; Shu, H.; Zhang, Y.H.; Yang, H.M.; Yang, L.J. Formation and decomposition of NH4HSO4 during selective catalytic reduction of NO with NH3 over V2O5-WO3/TiO2 catalysts. *Fuel Process. Technol.* **2016**, *150*, 141–147. [CrossRef]
30. Alemany, L.J.; Berti, F.; Busca, G.; Ramis, G.; Robba, D.; Toledo, G.P.; Trombetta, M. Characterization and composition of commercial V_2O_5&z. sbnd; WO_3&z. sbnd; TiO_2 SCR catalysts. *Appl. Catal. B* **1996**, *10*, 299–311.
31. Long, R.Q.; Yang, R.T. Characterization of Fe-ZSM-5 catalyst for selective catalytic reduction of nitric oxide by ammonia. *J. Catal.* **2000**, *194*, 80–90. [CrossRef]

32. Machida, M.; Murata, Y.; Kishikawa, K.; Zhang, D.; Ikeue, K. On the reasons for high activity of CeO_2 catalyst for soot oxidation. *Chem. Mater.* **2008**, *20*, 4489–4494. [CrossRef]
33. Kwon, D.W.; Nam, K.B.; Hong, S.C. The role of ceria on the activity and SO_2 resistance of catalysts for the selective catalytic reduction of NO_x by NH_3. *Appl. Catal. B Environ.* **2015**, *196*, 37–44. [CrossRef]